

<p><b>SDC</b> <b>SOLENOIDAL DETECTOR NOTES</b></p>
--

**PATTERN RECOGNITION IN A SILICON AND SCINTILLATING  
FIBER SDC TRACKING SYSTEM II**

David L. Adams  
*Rice University*

February 7, 1992

## Pattern Recognition in a Silicon and Scintillating Fiber SDC Tracking System II

David L. Adams  
Rice University

February 7, 1992

A silicon and scintillating fiber design for the SDC tracking system has been simulated at luminosities up to 10X the SSC design value. Results are presented for occupancies, efficiencies and resolutions of isolated muons and electrons. Little or no performance degradation is found at the highest luminosities.

### Introduction

One of the most basic requirements for an SSC tracking system is the ability to find and reconstruct isolated tracks especially electrons and muons. Ideally the system will retain this capability over the full luminosity range of the supercollider. One is naturally led to a design incorporating detection elements that are both fast and fine-grained. Consequently, we have simulated a system which uses silicon strips near the interaction point and scintillating fibers outside. We report results for a study involving leptonic decays of a 300 GeV Higgs boson. This work is an extension of that reported in an earlier SDC note [1]. Here we have performed runs with higher luminosities, have generated three times as many interesting leptons in each run and have made minor improvements to the track-finding algorithms.

### Detector

The simulated detector includes the silicon and scintillating fiber detectors, the beam pipe and the solenoid. The material outside the tracking system such as the calorimeter is not included. Tracks are stopped when they reach a radius of 225 cm or  $z = \pm 450$  cm. The solenoid is the standard default for the SDC simulation package SDCSIM. The silicon and fiber tracking systems are very similar to those described in the first-round conceptual design reports [2,3]. The silicon geometry and response is defined by the SDCSIM package ST and the geometry setup file is `st_descscope3.kumac` which is listed in appendix C of reference 1. Note that this geometry corresponds to design #2 in the draft silicon CDR [2] with the barrel-disk transition at  $45^\circ$ . The scintillating fiber geometry and response are defined by the SDCSIM package SF with geometry input file `sf_optc8.dat` which is included here as appendix A. In this geometry, all three outer cylindrical superlayers include stereo layers while in the previous study, this was true only for the

outermost superlayer. The active parts of the silicon and scintillating fiber systems are shown in figure 1.

The relevant part of the detector is the region  $|\eta| < 0.9$  which is covered by barrels only (no disks) by both tracking systems. We have concentrated on this region because our track-finding software is not yet working for disks. In this region, there are eight double-sided layers of silicon: one side with strips measuring  $r\phi$  and the other with 5 mrad stereo. The innermost layer is at 9 cm and the outermost at 36 cm. The layers have a few small gaps in  $z$  between wafers. The fiber system includes five superlayers with C1 at the outermost radius of 165 cm and C5 innermost at 75 cm. All superlayers include four adjacent layers of axial fibers with quarter-fiber offsets between them. The outer three superlayers (C1, C2 and C3) also each include two double layers of stereo fibers with opposite orientation and a stereo angle of  $15^\circ$ .

The light in the scintillating fibers is assumed to move at a constant speed (20 cm/ns) down the fiber and if it reaches the readout end of the fiber inside a specified time gate, then a digitization may be produced. For this study and the previous one, the time gate extends from 9 to 31 ns. This gate could be narrowed and still accept all prompt tracks for any given layer especially the shorter ones but the software (SF) presently uses the same gate for all superlayers. On the other hand, SF also does not include dispersion in the speed of propagation down the scintillating and optical fibers and this may require us to increase the gate by as much as 5 ns. Our choice for the width of this gate is probably within 30% of the value that will finally be used for the central barrels.

There are a series of parameters read in from the SF geometry file (appendix A) that determine the response of the fibers and electronics. These are set so that 6.4 photoelectrons are produced if a minimum ionizing par-

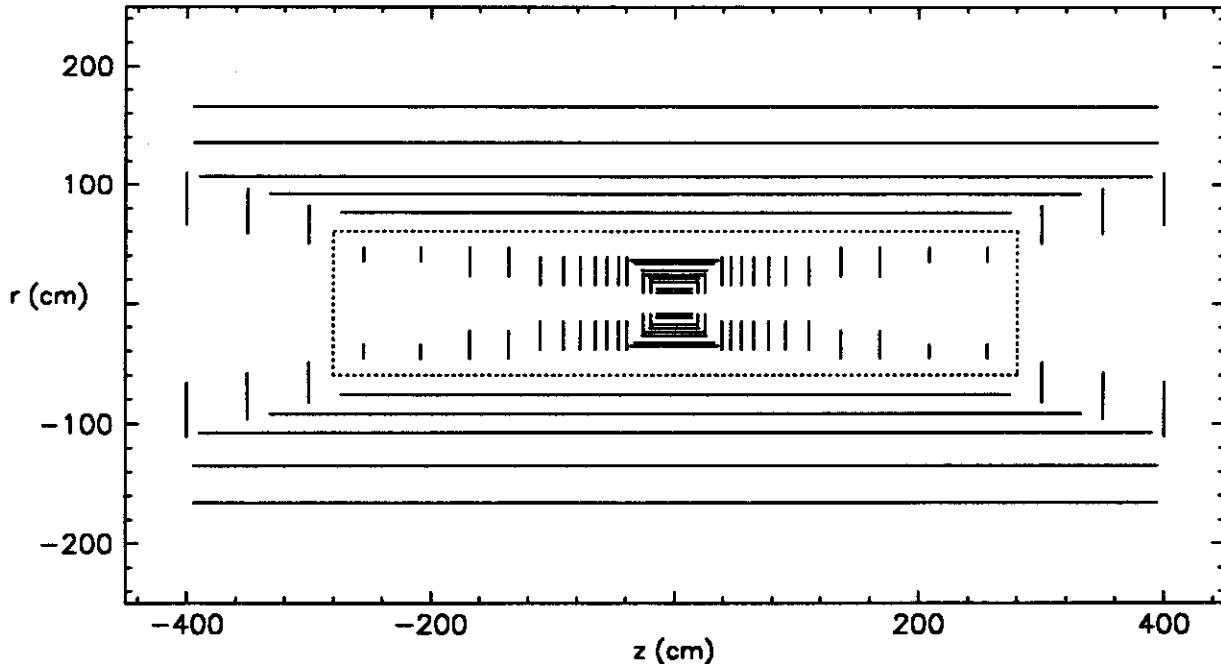


Figure 1. The SDC tracking system used in this study. The dotted lines show the boundary between the silicon and scintillating fiber systems. This study only makes use of the barrel detectors.

particle crosses the center of the fiber near the readout fiber and 2.9 are produced if it crosses 400 cm away. The actual number of photoelectrons produced is randomly selected from a Poisson distribution and a fiber is digitized (i.e. recorded as being hit) if this number is at least one.

#### Event Generation

We generated a series of runs each containing 100 primary events with varying numbers of background events to simulate different SSC luminosities. The primary events were 300 GeV Higgs decaying into two Z-bosons with one Z decaying into two muons and the other into two electrons. These were generated using Isajet with the control file listed in Appendix B. The events were filtered to select only those for which all four leptons had  $|\eta| < 0.85$ .

Background was generated using Pythia QCD inelastic events in all crossings from four before the interesting event through two after. The SSC design luminosity of  $10^{33}/\text{cm}^2/\text{sec}$  was simulated with an average of 1.6 such events per crossing where the actual number of generated events was selected from a Poisson distribution. Other luminosities were obtained by scaling this average. The vertex position of each generated event was independently selected from a distribution

Gaussian in  $z$  with  $\sigma = 5\text{cm}$  and in  $x$  and  $y$  with  $\sigma = 5\mu\text{m}$ .

#### Occupancies

After generating events and tracking them through the detector, the occupancy was measured separately for

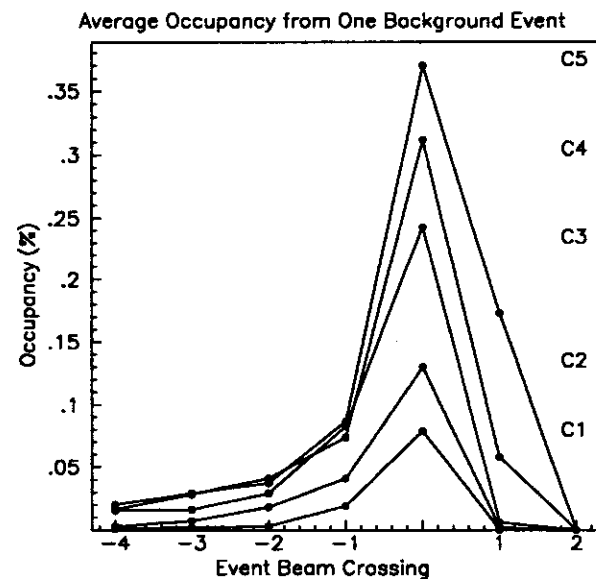


Figure 2. Occupancy contribution from one background event in different beam crossings.

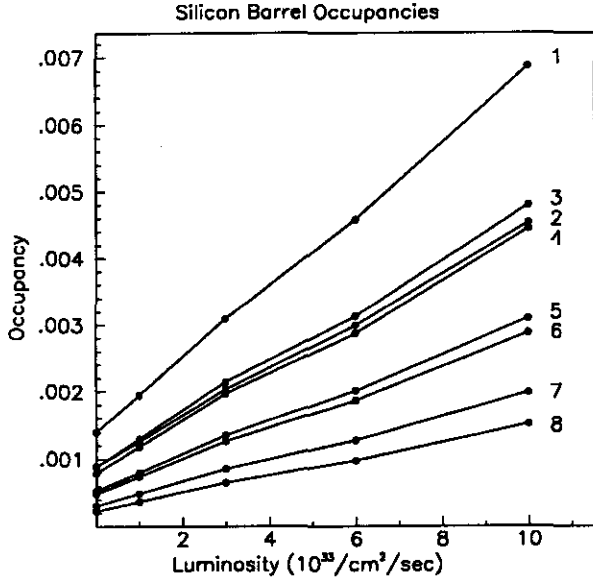


Figure 3. Silicon occupancies as a function of luminosity.

layer	L=0	L=L <sub>0</sub>	L=3L <sub>0</sub>	L=6L <sub>0</sub>	L=10L <sub>0</sub>
1	0.00140	0.00194	0.00309	0.00458	0.00687
2	0.00089	0.00126	0.00203	0.00299	0.00454
3	0.00088	0.00130	0.00214	0.00313	0.00480
4	0.00079	0.00118	0.00196	0.00287	0.00445
5	0.00053	0.00080	0.00135	0.00200	0.00310
6	0.00048	0.00074	0.00126	0.00186	0.00288
7	0.00031	0.00049	0.00085	0.00127	0.00198
8	0.00023	0.00037	0.00065	0.00097	0.00151

Table 1. Average occupancies in each of the silicon barrel layers for our central  $H \rightarrow ZZ \rightarrow 2\mu 2e$  events with different background luminosities ( $L_0 = 10^{33}/\text{cm}^2/\text{sec}$ ). Layers are numbered starting at the inside.

each superlayer. The occupancy is defined to be the fraction of channels which have been digitized. Figure 2 shows the average occupancy contributed by single background events in different beam crossings. The Higgs occupancies for each of the silicon layers are given in figure 3 and table 1 and the scintillating fiber occupancies appear in figure 4 and table 2.

### Track Reconstruction

Track finding and reconstruction were performed with the program TRF (SDCSIM package TR). TRF uses a road-following technique with a road map provided by the user at run time. Tracks were found in three ways: in silicon only, fibers only and in the combined system. The combined fitting was done by extrapolating the silicon tracks in to the fibers. In all cases tracks were

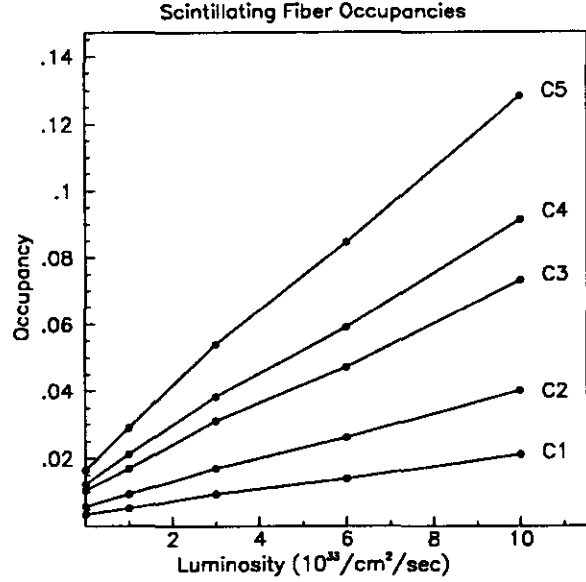


Figure 4. Scintillating fiber occupancies as a function of luminosity.

layer	L=0	L=L <sub>0</sub>	L=3L <sub>0</sub>	L=6L <sub>0</sub>	L=10L <sub>0</sub>
C1	0.0035	0.0054	0.0095	0.0140	0.0211
C2	0.0058	0.0095	0.0170	0.0261	0.0400
C3	0.0106	0.0170	0.0310	0.0471	0.0731
C4	0.0124	0.0212	0.0382	0.0590	0.0914
C5	0.0165	0.0290	0.0539	0.0846	0.1283

Table 2. Occupancies for each of the scintillating fiber superlayers for our central  $H \rightarrow ZZ \rightarrow 2\mu 2e$  events at different background luminosities ( $L_0 = 10^{33}/\text{cm}^2/\text{sec}$ ). Superlayers are labeled from outermost C1 to innermost C5.

found and fitted with a radial vertex constraint imposed and then were refit without the vertex constraint.

### Analysis

The performance of the tracking system is evaluated using the leptons from the Higgs decay. There are 200 of each in each of our runs. We define candidate tracks to be the subset of these that intercept all the silicon barrels and have  $p_T$  greater than 5 GeV/c. Approximately 10% of the generated leptons did not meet these criteria most because they missed some of the silicon detectors due to fluctuations in the  $z$ -position of the vertex.

Each of the reconstructed tracks is compared with each Monte Carlo track by calculating the match chi-square defined by:

$$\chi_M^2 = \sum_{i,j} (T_i^{rec} - T_i^{mc}) E_{ij}^{-1} (T_j^{rec} - T_j^{mc})$$

where  $T^{rec}$  and  $T^{mc}$  are, respectively, the reconstructed and Monte Carlo track vectors and  $E$  is the error matrix for the reconstructed track. Each reconstructed track is assigned to the Monte Carlo track for which the match chi-square is smallest. If two reconstructed tracks would be assigned to the same Monte Carlo track, then the one with larger match chi-square is left unassigned. Each of the Monte Carlo tracks is said to be "found" if a reconstructed track is assigned to it.

Two kinds of efficiencies are defined. The track finding efficiency is the fraction of candidate tracks which have been found as defined in the previous paragraph. The more restrictive track reconstruction efficiency is defined to be the fraction of candidate tracks which have been found and are well reconstructed. Tracks are said to be well reconstructed if they have a match chi-square below some cutoff value. In the present work the cutoff value is always taken to be 100.

Resolutions are defined to be the root-mean-square (RMS) difference between reconstructed and Monte Carlo track parameters. We have adopted this definition for resolutions rather than fitting with a Gaussian in order to be sensitive to tails of the distributions which might be expected to appear at high luminosities. The "well reconstructed" tracks are used to calculate the resolutions.

## Results

The track reconstruction was quite successful for silicon alone and silicon plus fibers at all luminosities. The track-finding in the fibers alone was very time consuming and we only present results at zero and design luminosities mostly to indicate the contribution to the resolutions. Our track-fitting algorithm does not account for multiple scattering or bremsstrahlung and consequently is not optimized for finding or fitting electrons. We draw conclusions from the results for muons presenting electron data for comparison. Work is in progress to optimize electron reconstruction.

The measured efficiencies are shown in figure 5. The muon track-finding and reconstruction efficiencies are around 99% and show no degradation with increasing luminosity. The electron efficiencies are lower but also independent of luminosity.

We see very few fake tracks. No more than two reconstructed tracks were unmatched in any run corresponding to a rate less than 0.02/crossing. There are significant numbers of tracks with match chi-square above our limit of 100 but the rate of such tracks does not increase very rapidly with increasing luminosity. Many of these tracks correspond to the missing electrons.

Resolutions for all the primary track parameters have been measured and are presented for both muons and electrons. All are plotted as a function of luminosity from zero to 10X the SSC design value. Figure 6 shows the transverse momentum resolution with and without a radial vertex constraint. Both systems (silicon and scintillating fiber) make important contributions to the overall resolution which is  $\Delta p_T/p_T^2 = 0.15$  (TeV/c)<sup>-1</sup> with the vertex constraint and 0.17 (TeV/c)<sup>-1</sup> without. Figure 7 shows the resolution in the transverse direction of motion at the point of closest approach. Again both systems contribute significantly to give a value better than 0.1 mrad with or without a vertex constraint. Figures 8 and 9 show the resolution in the position at closest approach. The impact parameter is measured to 20  $\mu\text{m}$  with the silicon alone improving to 9  $\mu\text{m}$  when the outer system is added. The z-resolution improves from 3 mm to 1 mm going from silicon alone to silicon plus fibers. Finally, the dip angle ( $dz/ds_T$ ) resolution is shown in figure 10. Most of the resolution comes from the outer system with the value improving from 0.011 to 0.0006 when the fibers are added.

## Conclusions

The SDC tracking system described here is a very powerful one for finding and reconstructing isolated muons. The efficiency is very high and the resolutions easily meet the SDC design goals. Most important, this statement remains valid for luminosities up to 10X the SSC design value (i.e. at 10<sup>34</sup> cm<sup>-2</sup>s<sup>-1</sup>). This follows from the fine granularity and consequent low occupancies in the silicon and scintillating fiber systems. The corresponding electron efficiencies and resolutions are somewhat degraded because of the significant amount of material in the tracking system and future studies will attempt to compensate for the material in the reconstruction and consider layouts with different material distributions.

## References

1. D. L. Adams, G. Eppley and J. Skeens, "Pattern Recognition in a Silicon and Scintillating Fiber SDC Tracking System," SDC-91-131 (Nov. 1991).
2. "Silicon Tracking Conceptual Design Report 1991," SDC-91-133 (Nov. 1991).
3. Fiber Tracking Group, "Conceptual Design Scintillating Fiber Outer Tracker," (Nov. 1991).

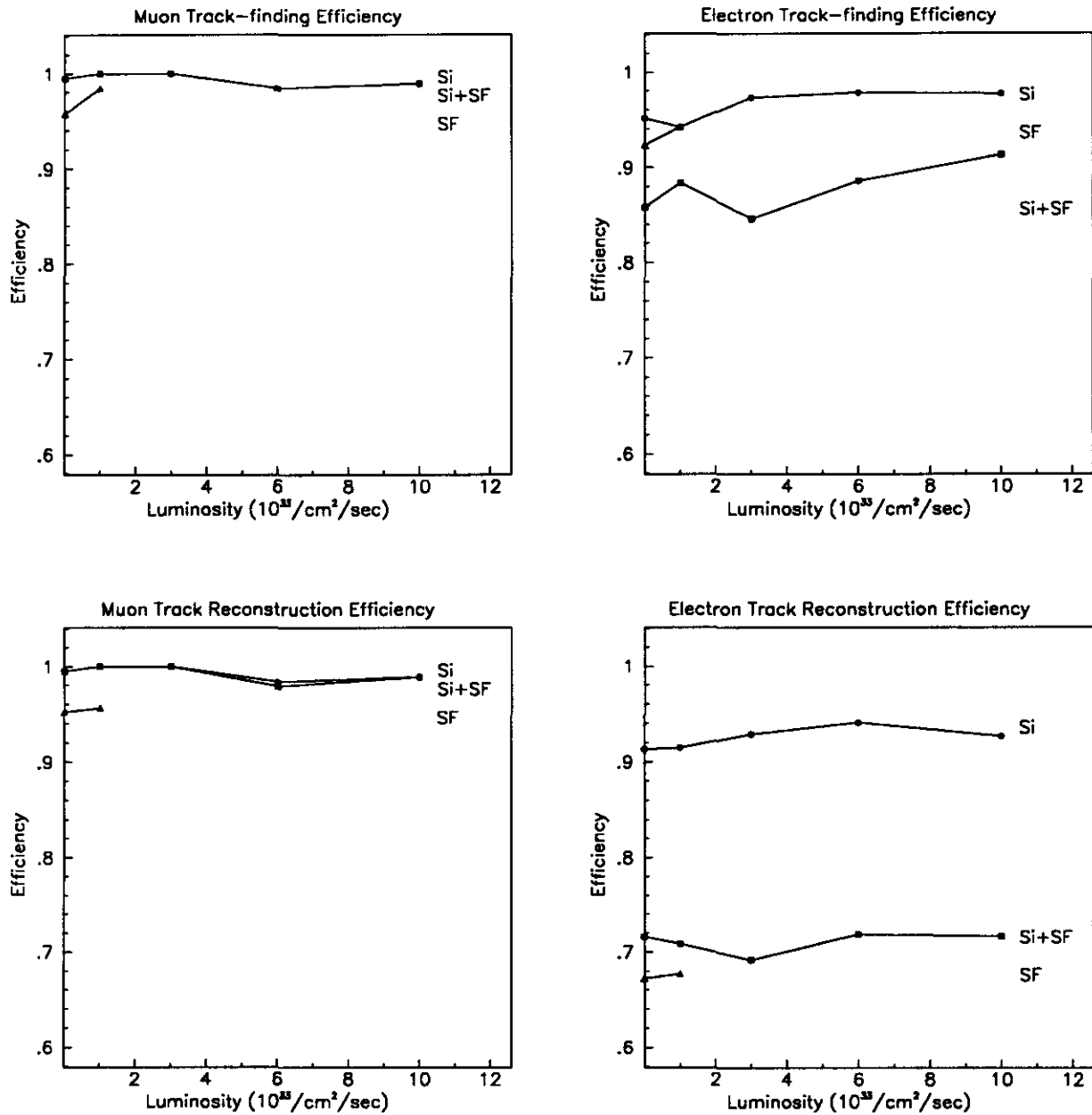


Figure 5. Track-finding and reconstruction efficiencies for muons and electrons. Each plot shows results at all luminosities for silicon alone (Si) and silicon extrapolated into the fibers (Si+SF). Fibers alone (SF) are shown for low luminosity. Most of the muon Si+SF points fall on top of the Si points indicating that no tracks are lost extrapolating into the fiber system.

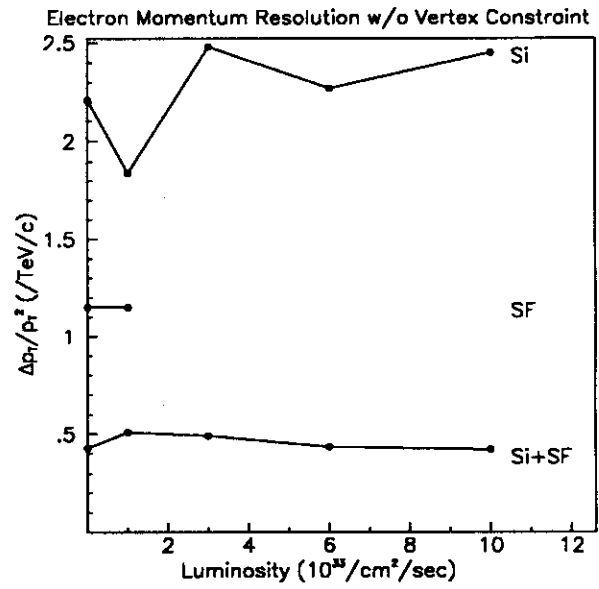
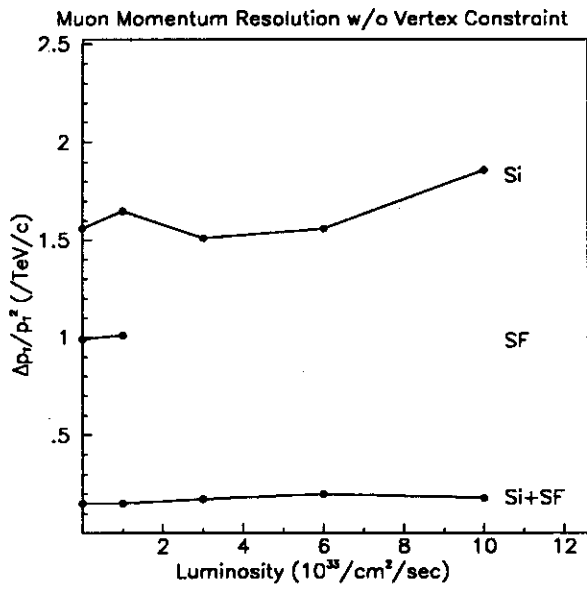
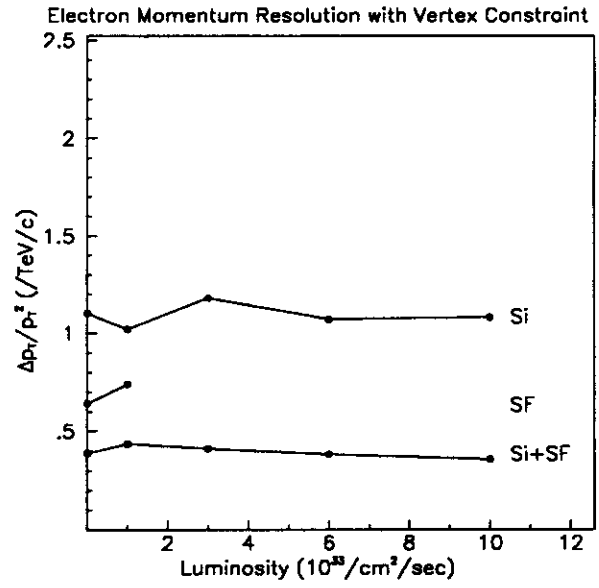
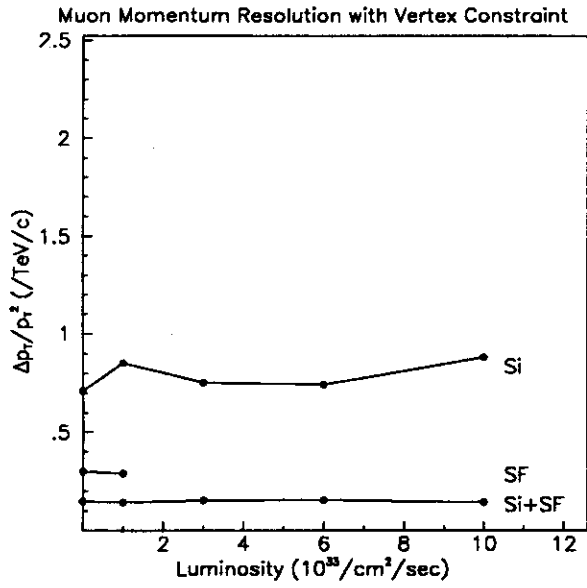


Figure 6. Transverse momentum resolution as a function of luminosity. Muons are on the left and electrons on the right. The top figures include a vertex constraint while those on the bottom do not. Results are shown for silicon alone (Si), fibers alone (SF) and the combined system (Si+SF).

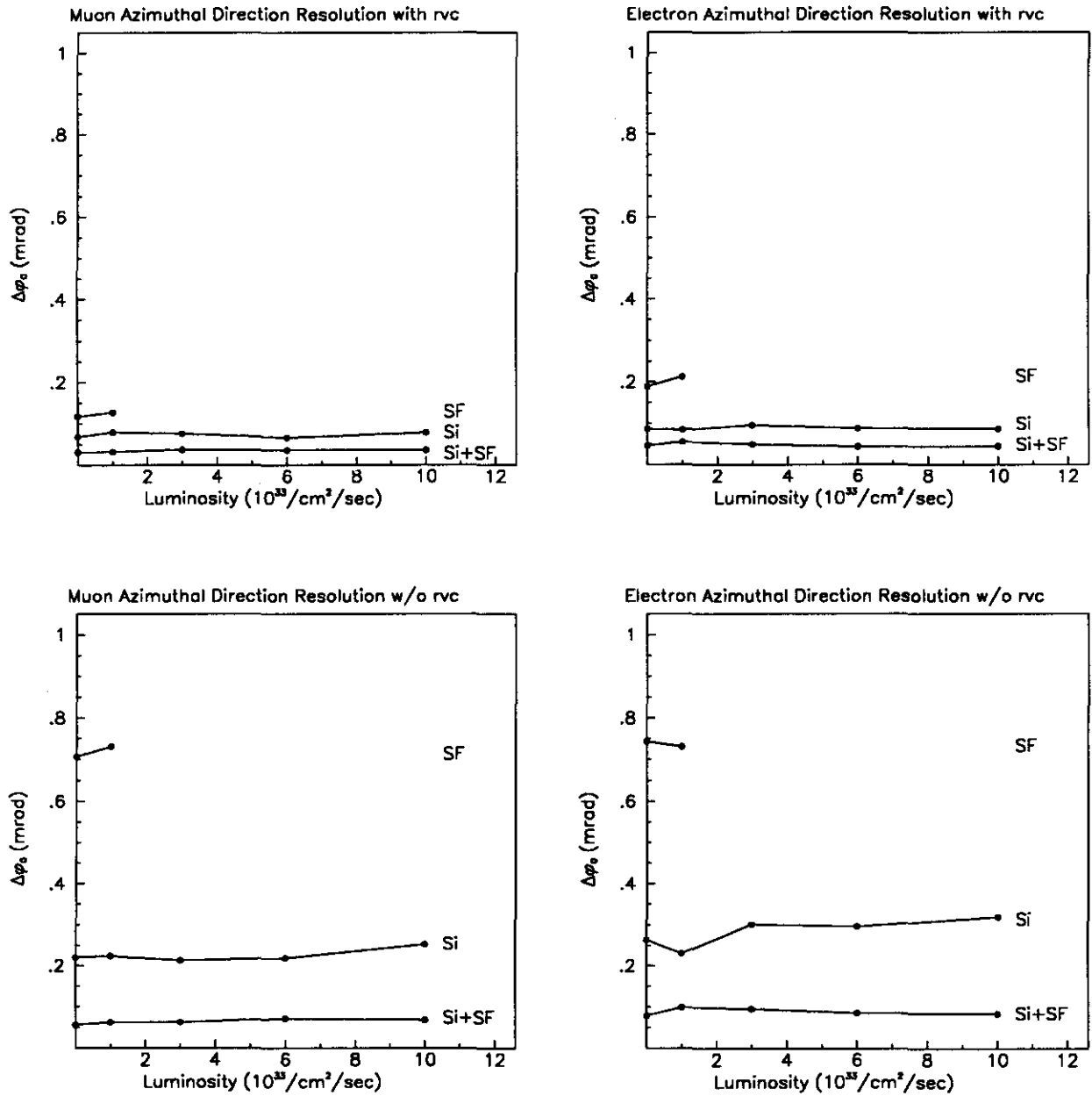


Figure 7. Resolution of the initial transverse direction of motion as a function of luminosity. Muons are on the left and electrons on the right. The top plots include a vertex constraint while those on the bottom do not. Results are shown for silicon alone (Si), fibers alone (SF) and the combined system (Si+SF).

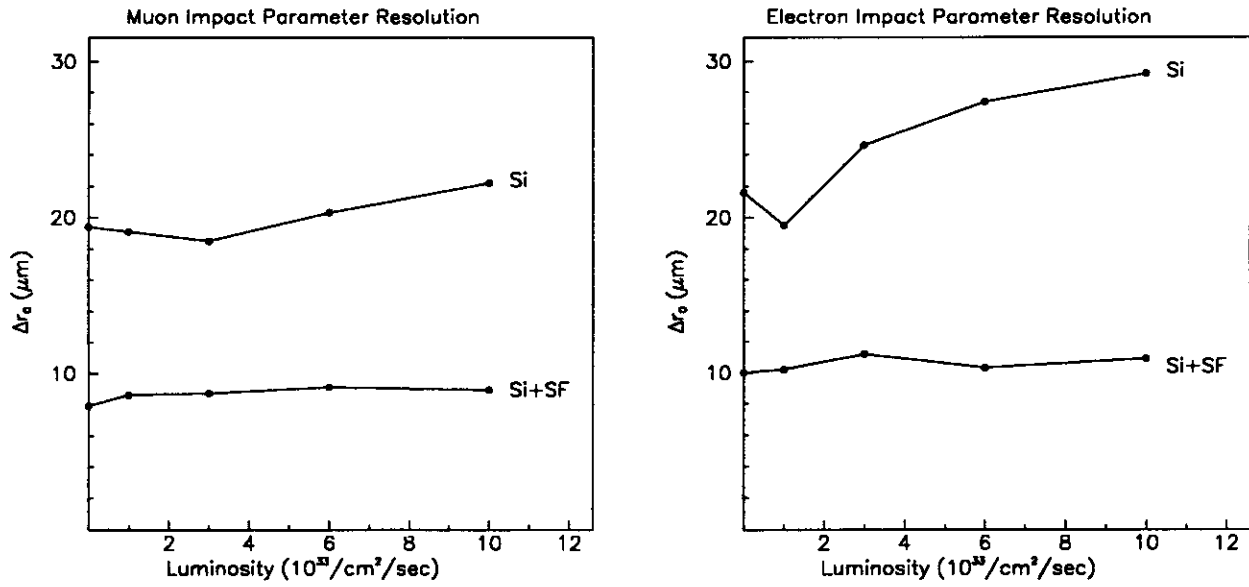


Figure 8. Impact parameter (transverse distance of closest approach) resolution as a function of luminosity. Muons are on the left and electrons on the right. Results are shown for silicon alone (Si) and silicon plus fibers (Si+SF).

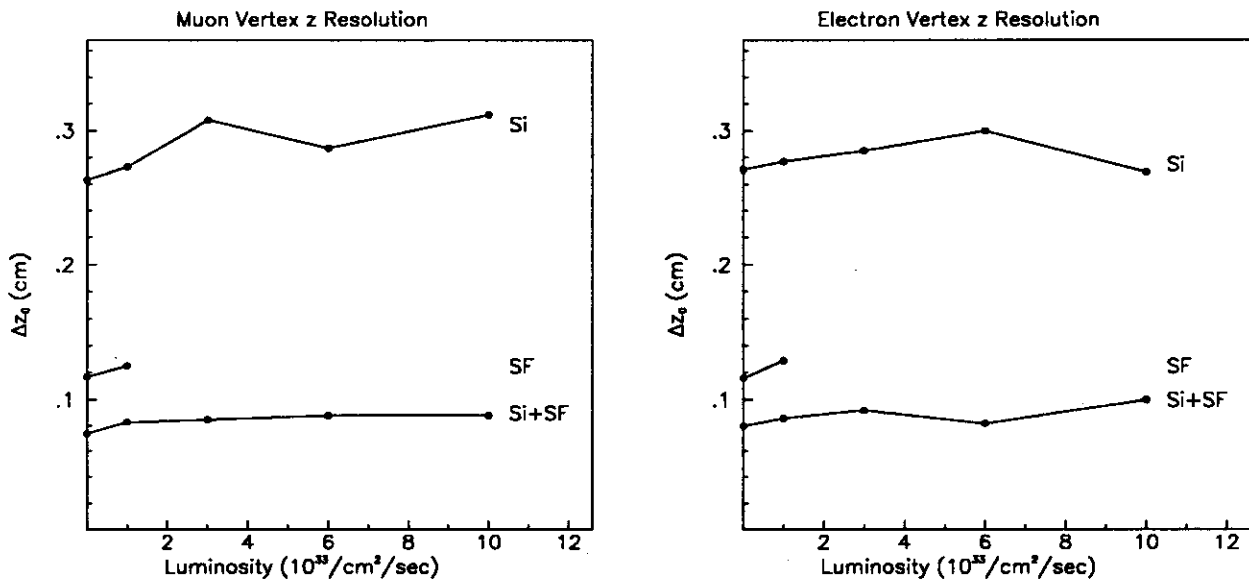


Figure 9. Vertex z-resolution as a function of luminosity. Muons are on the left and electrons on the right. Results are shown for silicon alone (Si), fibers alone (SF) and the combined system (Si+SF).

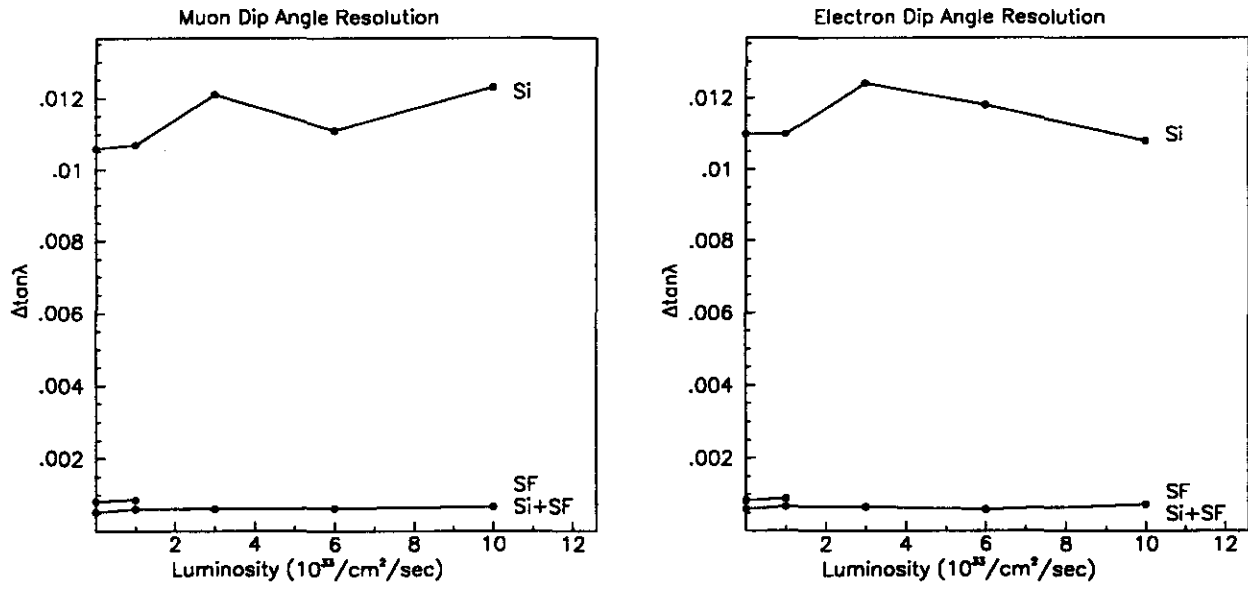


Figure 10. Dip angle resolutions as a function of luminosity. Muons are on the left and electrons on the right. Results are shown for silicon alone (Si), fibers alone (SF) and the combined system (Si+SF).

Appendix A

```

SF.DAT
/
/
/
03NOV91 dia - Fix bug: The C3 volumes were both offset by 5 cm so that
optc9
/
/
23NOV91 dia - Fix bug: the readout for the new stereo layers was always
optc7
/
/
21NOV91 dia - Add stereo to C2 and C3. Note that the current CDR includes
stereo in C3 but not C2. All layers are 15 degree stereo:
r THRU (deg) alpha (rad/cm)
165 15 0.00161
136 15 0.00197
108 15 0.00248
/
/
02NOV91 dia - The previous version of this file was bad. A mistake in the
optc5
light propagation speed => no fiber digitizations.
/
/
31OCT91 dia - modify digitization parameters -- I decreased the lightoutput
and fixed the timing so that we no longer lose 0.5 ns on the
fast end
/
31OCT91 dia - fix fiber spacing in C2 to be 0.087 instead of 0.089
Created 28 OCT 91 dia.
/
/
Describes FPG option C as circulated by D. Koltick. See figure in
DLA log II-43. Layer spacings are on II-34.
Modified to reflect new drawings circulated 30OCT91. See drawing and
layer positions on II-46.
/
/
Contains a description of a scintillating fiber tracking detector for
use with SSC simulations. A series of volumes are defined by giving names
for the shape and then the size, position and orientation.
The units are cm and radians.
/
/
The line beginning with 'digit' is followed with two lines setting the
parameters used in the digitization:
MDOTIM = fraction of photons detected, reflected = 1 - cos(theta)
PHOTEN = attenuation length in the scintillating fiber
ATTOPT = attenuation in optical fiber and couplings
QUANEF = quantum efficiency of the photodetector
VEIG = speed of the signal in the fiber (cm/s)
Defaults are provided if these lines are missing; they are:
1 16.0 20.0 16.0
1 .7 0.030 1000.0 0.5 0.6 20.e9
The following parameters give 10.2 photons at the near end of a fiber and
4.5 at 4 meters. The timing is set to accept all prompt particles and has
5 ns of slop on the slow end.
digitization parameters
1 16.0 21.0 22.0 ; see log II-48
0.50e7 0.030 500.0 0.5 0.8 20.0E9 ; see II-49
/
mother ; description of mother volume
170.0, 420.0 ; outer radius and half-length
/
/
***** C1 *****
/
cylinder ; volume shape
165.24 166.16 395. ; min radius, max radius, length (cm)
0. 0. -197.5 ; location of center of cylinder
8 ; number of fiber layers
1, -1 ; fiber shape, readout
0.087, 0.083, 0.0 ; fiber spacing (cm), width (cm), not used
165.49, 165.49, 0.00, 0.00000 ; r0, r, offset, stereo slope (rad/cm)
1, -1 ; fiber shape, readout
0.087, 0.083, 0.0 ; fiber spacing (cm), width (cm), not used
165.49, 165.57, 0.50, 0.00000 ; r0, r, offset, stereo slope (rad/cm)
1, -1 ; fiber shape, readout
0.087, 0.083, 0.0 ; fiber spacing (cm), width (cm), not used
165.49, 165.67, 0.25, 0.00000 ; r0, r, offset, stereo slope (rad/cm)
1, -1 ; fiber shape, readout
0.087, 0.083, 0.0 ; fiber spacing (cm), width (cm), not used
165.49, 165.75, 0.75, 0.00000 ; r0, r, offset, stereo slope (rad/cm)
1, -1 ; fiber shape, readout
0.087, 0.083, 0.0 ; fiber spacing (cm), width (cm), not used
165.85, 165.85, 0.00, 0.00161 ; r0, r, offset, stereo slope (rad/cm)
1, 1 ; fiber shape, readout
0.087, 0.083, 0.0 ; fiber spacing (cm), width (cm), not used
165.85, 165.93, 0.50, 0.00161 ; r0, r, offset, stereo slope (rad/cm)
1, -1 ; fiber shape, readout
0.087, 0.083, 0.0 ; fiber spacing (cm), width (cm), not used
166.03, 166.03, 0.00, -0.00161 ; r0, r, offset, stereo slope (rad/cm)
1, 1 ; fiber shape, readout
0.087, 0.083, 0.0 ; fiber spacing (cm), width (cm), not used
166.03, 166.11, 0.50, -0.00161 ; r0, r, offset, stereo slope (rad/cm)
/
/
cylinder ; volume shape
165.24 166.16 395. ; min radius, max radius, length (cm)
0. 0. -197.5 ; location of center of cylinder
8 ; number of fiber layers
1, 1 ; fiber shape, readout
0.087, 0.083, 0.0 ; fiber spacing (cm), width (cm), not used
165.49, 165.49, 0.00, 0.00000 ; r0, r, offset, stereo slope (rad/cm)
1, 1 ; fiber shape, readout
0.087, 0.083, 0.0 ; fiber spacing (cm), width (cm), not used
165.49, 165.57, 0.50, 0.00000 ; r0, r, offset, stereo slope (rad/cm)
1, 1 ; fiber shape, readout
0.087, 0.083, 0.0 ; fiber spacing (cm), width (cm), not used
165.49, 165.75, 0.75, 0.00000 ; r0, r, offset, stereo slope (rad/cm)
1, 1 ; fiber shape, readout
0.087, 0.083, 0.0 ; fiber spacing (cm), width (cm), not used
165.85, 165.85, 0.00, 0.00161 ; r0, r, offset, stereo slope (rad/cm)
1, 1 ; fiber shape, readout
0.087, 0.083, 0.0 ; fiber spacing (cm), width (cm), not used
165.85, 165.93, 0.50, 0.00161 ; r0, r, offset, stereo slope (rad/cm)
1, 1 ; fiber shape, readout
0.087, 0.083, 0.0 ; fiber spacing (cm), width (cm), not used
166.03, 166.03, 0.00, -0.00161 ; r0, r, offset, stereo slope (rad/cm)
1, 1 ; fiber shape, readout
0.087, 0.083, 0.0 ; fiber spacing (cm), width (cm), not used
166.03, 166.11, 0.50, -0.00161 ; r0, r, offset, stereo slope (rad/cm)
/
/
***** C2 *****
/
cylinder ; volume shape
135.34 136.26 395. ; min radius, max radius, length (cm)
0. 0. -197.5 ; location of center of cylinder
8 ; number of fiber layers
1, -1 ; fiber shape, readout
/
/
***** C3 *****
/
cylinder ; volume shape
107.42 108.34 390. ; min radius, max radius, length (cm)
0. 0. -195.0 ; location of center of cylinder
8 ; number of fiber layers
1, -1 ; fiber shape, readout
0.087, 0.083, 0.0 ; fiber spacing (cm), width (cm), not used
107.67, 107.67, 0.00, 0.00000 ; r0, r, offset, stereo slope (rad/cm)
1, 1 ; fiber shape, readout
0.087, 0.083, 0.0 ; fiber spacing (cm), width (cm), not used
107.67, 107.75, 0.50, 0.00000 ; r0, r, offset, stereo slope (rad/cm)
1, -1 ; fiber shape, readout
0.087, 0.083, 0.0 ; fiber spacing (cm), width (cm), not used
107.67, 107.85, 0.25, 0.00000 ; r0, r, offset, stereo slope (rad/cm)
1, 1 ; fiber shape, readout
0.087, 0.083, 0.0 ; fiber spacing (cm), width (cm), not used
107.67, 107.93, 0.75, 0.00000 ; r0, r, offset, stereo slope (rad/cm)
1, -1 ; fiber shape, readout
0.087, 0.083, 0.0 ; fiber spacing (cm), width (cm), not used
108.03, 108.03, 0.00, 0.00248 ; r0, r, offset, stereo slope (rad/cm)
1, 1 ; fiber shape, readout
0.087, 0.083, 0.0 ; fiber spacing (cm), width (cm), not used
108.03, 108.11, 0.50, 0.00248 ; r0, r, offset, stereo slope (rad/cm)
1, -1 ; fiber shape, readout
0.087, 0.083, 0.0 ; fiber spacing (cm), width (cm), not used
108.21, 108.21, 0.00, -0.00248 ; r0, r, offset, stereo slope (rad/cm)
1, 1 ; fiber shape, readout
0.087, 0.083, 0.0 ; fiber spacing (cm), width (cm), not used
108.21, 108.29, 0.50, -0.00248 ; r0, r, offset, stereo slope (rad/cm)
/
/
cylinder ; volume shape
107.42 108.34 390. ; min radius, max radius, length (cm)
0. 0. -195.0 ; location of center of cylinder
8 ; number of fiber layers
1, 1 ; fiber shape, readout
0.087, 0.083, 0.0 ; fiber spacing (cm), width (cm), not used
107.67, 107.67, 0.00, 0.00000 ; r0, r, offset, stereo slope (rad/cm)
1, 1 ; fiber shape, readout
0.087, 0.083, 0.0 ; fiber spacing (cm), width (cm), not used
107.67, 107.75, 0.50, 0.00000 ; r0, r, offset, stereo slope (rad/cm)
1, 1 ; fiber shape, readout
0.087, 0.083, 0.0 ; fiber spacing (cm), width (cm), not used
108.03, 108.03, 0.00, 0.00248 ; r0, r, offset, stereo slope (rad/cm)
1, 1 ; fiber shape, readout
0.087, 0.083, 0.0 ; fiber spacing (cm), width (cm), not used
108.03, 108.11, 0.50, 0.00248 ; r0, r, offset, stereo slope (rad/cm)
1, 1 ; fiber shape, readout
0.087, 0.083, 0.0 ; fiber spacing (cm), width (cm), not used
108.21, 108.21, 0.00, -0.00248 ; r0, r, offset, stereo slope (rad/cm)
1, 1 ; fiber shape, readout
0.087, 0.083, 0.0 ; fiber spacing (cm), width (cm), not used
108.21, 108.29, 0.50, -0.00248 ; r0, r, offset, stereo slope (rad/cm)
/
/
***** C4 *****
/
cylinder ; volume shape
91.47, 92.03, 332.0 ; min radius, max radius, length (cm)
0. 0. -166.0 ; location of center of cylinder
8 ; number of fiber layers
1, -1 ; fiber shape, readout
0.087, 0.083, 0.0 ; fiber spacing (cm), width (cm), not used
91.72, 91.72, 0.00, 0.00000 ; r0, r, offset, stereo slope (rad/cm)
1, 1 ; fiber shape, readout
0.087, 0.083, 0.0 ; fiber spacing (cm), width (cm), not used
91.72, 91.80, 0.50, 0.00000 ; r0, r, offset, stereo slope (rad/cm)
1, -1 ; fiber shape, readout
0.087, 0.083, 0.0 ; fiber spacing (cm), width (cm), not used
91.72, 91.90, 0.25, 0.00000 ; r0, r, offset, stereo slope (rad/cm)
1, -1 ; fiber shape, readout
/
/

```

